PCCP

PAPER

View Article Online
View Journal

Exploring the electrostatic energy landscape for tetraloop–receptor docking†

Cite this: DOI: 10.1039/c3cp53655f

Zhaojian He,‡[a] Yuhong Zhu‡[abc] and Shi-Jie Chen*[a]

Received 29th August 2013,
Accepted 12th November 2013

DOI: 10.1039/c3cp53655f

www.rsc.org/pccp

It has long been appreciated that Mg^{2+} is essential for the stabilization of RNA tertiary structure. However, the problem of quantitative prediction for the ion effect in tertiary structure folding remains. By using the virtual bond RNA folding model (Vfold) to generate RNA conformations and the newly improved tightly bound ion model (TBI) to treat ion–RNA interactions, we investigate Mg^{2+}-facilitated tetraloop–receptor docking. For the specific construct of the tetraloop–receptor system, the theoretical analysis shows that the Mg^{2+}-induced stabilizing force for the docked state is predominantly entropic and the major contribution comes from the entropy of the diffusive ions. Furthermore, our results show that Mg^{2+} ions promote tetraloop–receptor docking mainly through the entropy of the diffusive ions. The theoretical prediction agrees with experimental analysis. The method developed in this paper, which combines the theory for the (Mg^{2+}) ion effects in RNA folding and RNA conformational sampling, may provide a useful framework for studying the ion effect in the folding of more complex RNA structures.

Introduction

In RNA tertiary structure, a GNRA hairpin tetraloop (TL) interacts with a specific helix to form a tetraloop–receptor (TL–R) complex through long-range contacts.[1–3] A tetraloop–receptor complex is a frequently occurring basic building block for RNA tertiary structure. Therefore, understanding the mechanism of its formation can provide important insights into the physical mechanism for the assembly of tertiary folds. Because the formation of a tetraloop–receptor involves a significant build-up of RNA backbone charges, the folding driving force is intrinsically sensitive to the ionic conditions of the solution.[1,4–8]

Several recent experiments have uncovered a number of novel ion effects in the formation of a tetraloop–receptor motif.[1,5,9–23] Davis *et al.* used NMR to study the role of metal ions in stabilizing the tetraloop–receptor solution structure and found the stable native structure of the tetraloop–receptor complex formed under ionic conditions.[5] Qin *et al.* used site-directed spin labeling to explore the tetraloop–receptor conformational changes. The experimental data demonstrated that base unstacking is an intrinsic feature of the solution tetraloop–receptor complex formed in the presence of Mg^{2+}.[24] Meulen and Butcher studied the tetraloop–receptor folding in salt solution using isothermal titration calorimetry (ITC) and found a significant difference in the kinetic and thermodynamic profiles of the system when it's stabilized by K^+ *versus* Mg^{2+} ions.[23] The result further suggested that the tertiary folding in physiological conditions may involve a complex interplay between K^+- and Mg^{2+}-induced stabilization.[23] Downey and co-workers investigated the effect of pressure and cosolutes on the tetraloop–receptor docking using FRET (fluorescence resonance energy transfer)[10] and found that (a) hydrostatic pressure slightly destabilizes the GAAA tetraloop–receptor interaction and (b) increasing the nondenaturing cosolutes favors the formation of the tetraloop–receptor tertiary structure.

Motivated by the need to understand the conformational distribution and folding pathways, a series of FRET experiments have been performed for the tetraloop–receptor docking in the monovalent and multivalent solutions.[1,13,17,22,25–27] These single molecule experiments led to several important findings. One of the remarkable findings is the entropic effect as the dominant driving force for tetraloop–receptor docking.[25] In contrast to the entropic effect, with increasing [Mg^{2+}], the Mg^{2+}-induced changes of the activation enthalpy and the overall exothermicity for docking are both negligible.[22] Moreover, in the transition state, Mg^{2+}-induced tetraloop–receptor docking arises from reducing the entropic barrier and the overall entropic penalty for docking.[22] This conclusion contradicts the conventional notion that the ion-dependent folding stability comes from charge neutralization and the resultant reduction in Coulomb repulsion energy.[25,26,28–33]

The above experiments have provided useful results on the ion dependence of the docking enthalpy and entropy.[13,15–17,19,22,23,25,26]

[a] Department of Physics and Department of Biochemistry, University of Missouri, Columbia, MO 65211, USA. E-mail: chenshi@missouri.edu
[b] Department of Physics, Zhejiang University, Hangzhou, ZheJiang, 310027, China
[c] Department of Physics, Hangzhou Normal University, Hangzhou, ZheJiang, 310036, China

† Electronic supplementary information (ESI) available. See DOI: 10.1039/c3cp53655f

‡ These authors contributed equally to this work.

Inspired by the deep insights from the experimental findings, we here develop a theory to analyze the quantitative roles for the different components of the driving force for docking. The detailed mechanism for tetraloop–receptor docking is determined by the complex interplay between multiple factors, such as the electrostatic energy, the conformational entropy, the solvent polarization energy and the entropies of the bound and diffusive ions. The three-dimensional atomic structures of the free form (undocked) and the native form (docked) of the tetraloop–receptor complex have been experimentally determined.[34–40] These structures have provided invaluable information about the energetics of the folding of the tetraloop–receptor. However, to fully understand the forces that promote the formation of the structure, we need to go beyond the structures and understand the folding thermodynamics and kinetics of the system. This requires information about the free energy landscape of the complete conformational ensemble, including the conformational ensembles for the free and the docked states. In the present study, we investigate the full electrostatic free energy landscape of the tetraloop–receptor docking in Na^+ and Mg^{2+} mixed solution.

One of the extensively studied tetraloop–receptor systems in experiments (such as the single molecule FRET experiment) consists of three minimal elements: a GAAA tetraloop, an 11-nt receptor in a helix, and a 7-nt poly(U) loop/linker between the tetraloop and the receptor.[1,13,17,22,25–27] We choose the above minimal tetraloop–receptor construct as a paradigm system for our study. To generate the conformational ensemble, we sample the three-dimensional (3D) structures of the docked and the undocked tetraloop–receptor in using the virtual bond-based RNA folding model (Vfold model).[41–43] In the Vfold model, RNA virtual bonds (P–C_4–P bonds) are configured on a diamond lattice and RNA conformations are enumerated through 3D self-avoiding random walks of RNA virtual bonds on the diamond lattice. An advantage of the Vfold model is that it can treat chain connectivity and exclude volume interferences within a loop/junction and between loop and loop and between loop and helix. For each conformation of the tetraloop–receptor docked and undocked states, we use the tightly bound ion (TBI) model[44–49] to calculate the electrostatic free energy in a Mg^{2+} solution. The TBI model is a statistical mechanics-based polyelectrolyte theory that can treat ion fluctuation and correlation effects for counterions around a nucleic acid structure. For multivalent ions such as Mg^{2+} ions, whose correlation and fluctuation effects may be strong, the TBI theory leads to better predictions for the ion-effect in folding thermodynamics than mean-field theories such as the Poisson–Boltzmann equation.[44–49] Here we used a combined Vfold/TBI approach. A unique advantage of such a combined theory is its ability to predict (a) the full energy landscape and (b) the detailed ion dependence of each enthalpic and entropic component as determined from the conformation ensemble. Our results show that the dominant Mg^{2+}-induced driving force comes from the decrease in the entropic penalty of the diffusive ions upon docking and the increase of the compactness of the structures in the undocked conformational ensemble. The conclusion supports the experimental findings. Furthermore, we found that the Coulomb interaction also plays a (weaker) role in promoting the tetraloop–receptor docking. The theory–experiment agreement suggests that the new theoretical method here may be reliable and can be useful for further treatment of the ion-dependent folding of more complex RNA tertiary structures.

Methods and theory

We consider two states for the tetraloop–receptor system: the docked (F) and the undocked (U) state (see Fig. 1a). In the undocked state, the tetraloop is freely oriented. In the docked state, the tertiary interactions, such as the hydrogen binding and base staking, are stabilized between the docked tetraloop and receptor.[17,22] In our calculation, we focus on the ion-dependence of the electrostatic free energy landscape. The tetraloop–receptor docking stability ΔG_{dock} is determined by the free energy difference between the docked (ΔG(F)) and the undocked (ΔG(U)) states:

$$\Delta G_{dock} = \Delta G(F) - \Delta G(U) \quad (1)$$

I. Structure model

In order to compare the theoretical predictions with the experimental data, we focus on an isolated GAAA tetraloop–receptor system (shown in Fig. 1a and b) similar to the one used in the experiment.[22,25,26] The only difference between our system and the experimental construct is that the DNA strand[22,25,26] connected to a biotin in the experiment is replaced by an RNA strand in our calculation, so the RNA duplex can be conveniently modeled as an A-form helix. Since the tetraloop–receptor docking site is relatively distant from the modified RNA duplex, we believe such a minor change would not cause notable changes to the results.

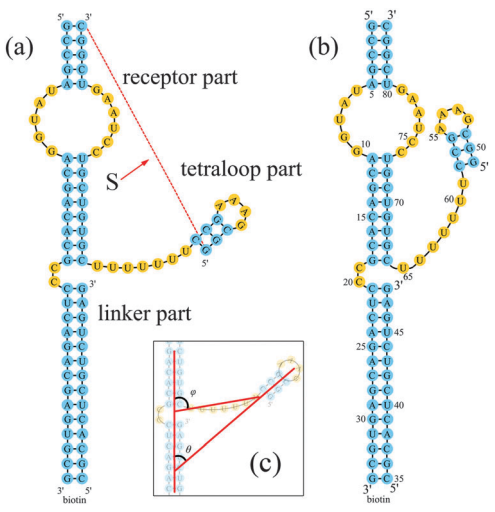

Fig. 1 The GAAA tetraloop–receptor system. The GAAA tetraloop and the receptor are connected by a U7 single-stranded linker. (a) The undocked state; (b) the docked state; (c) the definition of the structural parameters θ and ϕ.

The tetraloop–receptor system shown in Fig. 1 has three parts: the receptor, the linker and the tetraloop. The receptor part is formed by three long helices connected by an internal loop (receptor) and a short C_2 bulge loop. The linker part is a long U_7 flexible loop and the tetraloop part contains a GAAA tetraloop and the attached helix. One of the key issues for the structure modeling is how to sample the conformations for the docked and the undocked states. We use the experimentally determined structures (PDB ID: 1GID)[37] for the docked state. In the undocked state, we use the solution structure of the isolated tetraloop receptor (PDB ID: 1TLR)[38] for the receptor. Experimental structure determination shows that the tetraloop structure is unchanged before and after docking, so we used the same PDF structure (PDB ID: 1GID)[37] for the tetraloop for the docked and the undocked states. In both states, the flexible U_7 linker gives an ensemble of 3D conformations for the system. In the undocked state, the end of the U_7 linker connected to the tetraloop is free while the other end is fixed. As the U_7 loop samples the different conformations in the 3D space, the tetraloop attached to the linker moves accordingly in the 3D space. For the docked state, the tetraloop is fixed in the 3D space according to the PDB structure of the docked complex (PDB code: 1GID),[37] so both ends of the linker loop are fixed while the remaining five uracil nucleotides in the loop are flexible.

The Vfold model generates 2628 and 5 985 453 complete sets of conformations for the docked and undocked states, respectively. To classify the conformations, we define three structure parameters: the angle θ and the end-to-end distance S between the tetraloop helix and the receptor helix and the angle ϕ between the end-to-end vector and the receptor helix (see Fig. 1c).

Given the large number of conformations in the docked and undocked states, it is computationally impractical to consider all the conformations in the free energy calculation. We use the Monte Carlo method to sample conformations from the complete ensemble. To ensure the broad coverage of the conformational sampling for the docked and the undocked states, we uniformly divide the conformational space into 30 clusters according to the tetraloop–receptor distance S. In each cluster, we randomly select 30 conformations. For the docked state, the structure of the tetraloop–receptor complex is rigid (PDB ID: 1GID), therefore, we fix the distance S according to the experimentally determined structure of the complex. This leads to only one conformational cluster according to the S value. It is important to note that although there is only one cluster for the docked state, the tether loop connecting the tetraloop and the receptor can sample a large number of conformations. Our calculation for the docked state accounts for such a loop-generated conformational ensemble. To verify the validity of the conformational sampling, we perform four independent sets of Monte Carlo samplings to generate four groups of docked and undocked conformational ensembles. In each group, there are 900 conformations for the undocked states and 30 conformations for the docked case. Fig. 2c and d show subsets (30 structures) of the conformational ensembles for the undocked and the docked states.

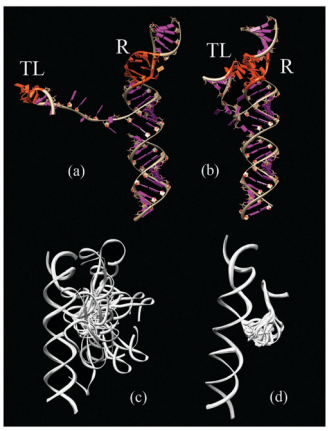

Fig. 2 Representative structures for (a) the undocked state and (b) the docked state. "TL" represents the GAAA tetraloop, and "R" represents the receptor, both the GAAA tetraloop and the receptor parts are marked in red. (c) and (d) show the conformational ensemble of the undocked and the docked states, respectively.

II. Electrostatic free energies of the tetraloop–receptor system

For each given tetraloop–receptor conformation, we use the tightly bound ion model (TBI)[44–49] to calculate the electrostatic free energy of the system. In contrast to other models, the TBI model has the advantage of accounting for the fluctuation in ion distribution and the correlations between multivalent ions in the close vicinity of the RNA surface. The model can also treat solvent polarization through the Generalized Born model (GB). See the (ESI†) for the details of the TBI model.

The TBI model gives the electrostatic free energy and ion binding properties for each tetraloop–receptor conformation. The Boltzmann-weighted average over all the conformations gives the net free energy, enthalpy and entropy of the docked and the undocked states respectively. More importantly, the model can provide quantitative results for the different energetic components, from which we determine the roles of the different forces in tetraloop–receptor docking. For each conformation j, we compute the total free energy $\Delta G_{\mathrm{T}}^{j}$ and its components: the Coulomb energy $\Delta G_{\mathrm{E}}^{j}$, the polarization energy $\Delta G_{\mathrm{P}}^{j}$ and the entropic free energy $\Delta G_{\mathrm{S}}^{j}$. For a given state M (the docked or undocked state), we calculate the free energy $\Delta G_{\mathrm{T}}(\mathrm{M})$ from the conformational ensemble (see ESI†).

The Coulomb energy $\Delta G_{\mathrm{E}}(\mathrm{M})$ and the polarization energy $\Delta G_{\mathrm{P}}(\mathrm{M})$ are given by the following equations:

$$\Delta G_{\mathrm{E}}(\mathrm{M}) = \frac{\sum_i \sum_j \Delta G_{\mathrm{E}}^{j}(\mathrm{M}) \cdot \mathrm{e}^{-\beta \Delta G_{\mathrm{T}}^{j}(\mathrm{M})}}{\sum_i \sum_j \mathrm{e}^{-\beta \Delta G_{\mathrm{T}}^{j}(\mathrm{M})}} \qquad (2)$$

and

$$\Delta G_{\mathrm{P}}(\mathrm{M}) = \frac{\sum_i \sum_j \Delta G_{\mathrm{P}}^{j}(\mathrm{M}) \cdot \mathrm{e}^{-\beta \Delta G_{\mathrm{T}}^{j}(\mathrm{M})}}{\sum_i \sum_j \mathrm{e}^{-\beta \Delta G_{\mathrm{T}}^{j}(\mathrm{M})}} \qquad (3)$$

where $\Delta G_{\mathrm{T}}^{j}(M)$ is the electrostatic free energy of the jth conformation in the ith cluster for state M. $\Delta G_{\mathrm{T}}^{j}(\mathrm{M})$ is calculated

from the TBI model (see ESI†). $\Delta G_{\mathrm{E}}^{j}(\mathrm{M})$ and $\Delta G_{\mathrm{P}}^{j}(\mathrm{M})$ are the Coulomb energy and the polarization energy of the jth conformation in the ith cluster in state M, respectively. $\Delta G_{\mathrm{E}}^{j}(\mathrm{M})$ and $\Delta G_{\mathrm{P}}^{j}(\mathrm{M})$ are calculated from the TBI model (see ESI†). The entropic free energy $\Delta G_{\mathrm{S}}(\mathrm{M})$ can be calculated as:

$$\Delta G_{\mathrm{S}}(\mathrm{M}) = \Delta G_{\mathrm{T}}(\mathrm{M}) - \Delta G_{\mathrm{E}}(\mathrm{M}) - \Delta G_{\mathrm{P}}(\mathrm{M}) \quad (4)$$

Here, the entropic free energy contains two parts: the first part is from the ion entropy $\Delta G_{\mathrm{S\_ion}}(\mathrm{M})$, including both the bound and the diffusive ions; the second part is from the conformational entropy $\Delta G_{\mathrm{S\_conf}}(\mathrm{M})$. The ion entropy can be calculated from the following equation:

$$\Delta G_{\mathrm{S\_ion}}(\mathrm{M}) = \frac{\sum_i \sum_j \Delta G_{\mathrm{S}}^{j}(\mathrm{M}) \cdot \mathrm{e}^{-\beta \Delta G_{\mathrm{T}}^{j}(\mathrm{M})}}{\sum_i \sum_j \mathrm{e}^{-\beta \Delta G_{\mathrm{T}}^{j}(\mathrm{M})}} \quad (5)$$

where $\Delta G_{\mathrm{S}}^{j}(\mathrm{M})$ is the entropic free energy of the jth conformation in the ith cluster in state M. Because the entropic free energy $\Delta G_{\mathrm{S}}^{j}(\mathrm{M})$ is for a fixed conformation, it represents the entropy from the ions (without the conformational entropy). The conformational entropy part can be obtained from the difference between the total entropic free energy and the ionic entropic free energy:

$$\Delta G_{\mathrm{S\_conf}}(\mathrm{M}) = \Delta G_{\mathrm{S}}(\mathrm{M}) - \Delta G_{\mathrm{S\_ion}}(\mathrm{M}) \quad (6)$$

The TBI model is used to calculate the electrostatic free energy for the docked and the undocked states in various $[Mg^{2+}]$ with the 0.1 M NaCl background at 37 °C (the experimental conditions).[22] The docking free energy, *i.e.*, the free energy difference between the docked and the undocked states, is determined from eqn (1).

Results

Our focus here is the [ion]-dependence of the free energy landscape. Fig. 3a shows the comparison of the experimental data[22] and our predicted results for the [ion]-dependence of the docking free energy ΔG_{dock}. The experimental data include both the electrostatic contribution $\Delta G_{\mathrm{dock}}^{\mathrm{E}}$ and the nonelectrostatic contribution $\Delta G_{\mathrm{dock}}^{\mathrm{NE}}$. In the solved tetraloop–receptor structure, the tetraloop binds by base stacking and hydrogen bonding to the minor groove of the receptor. The energies of base stacking and hydrogen bonding are not accounted for in the ion electrostatic calculations. Other nonelectrostatic interactions may include the nonpolar solvation energy. Our estimation of the change of the solvent accessible surface area between the docked and the undocked states a nonpolar solvation free energy of approximately 11 kcal mol^{-1} (see ESI†). The hydrogen bonding/base stacking network and the nonpolar solvation energy constitute the major portion of the nonelectrostatic free energy $\Delta G_{\mathrm{dock}}^{\mathrm{NE}}$.

Assuming the nonelectrostatic free energy $\Delta G_{\mathrm{dock}}^{\mathrm{NE}}$ to be independent of the ion concentration, we can extract $\Delta G_{\mathrm{dock}}^{\mathrm{NE}}$ as the difference between the total docking free energy ΔG_{dock} and the electrostatic free energy $\Delta G_{\mathrm{dock}}^{\mathrm{E}}$ at any ion concentration as the reference state:[45] $\Delta G_{\mathrm{dock}}^{\mathrm{NE}} = \Delta G_{\mathrm{dock}} - \Delta G_{\mathrm{dock}}^{\mathrm{E}}$. Here ΔG_{dock} is the experimental docking free energy at the reference ionic conditions and $\Delta G_{\mathrm{dock}}^{\mathrm{E}}$ is calculated from our TBI model. Choosing 0.5 mM $Mg^{2+}$and 100 mM Na^{+} mixed solution at 37 °C as the reference solution conditions, $\Delta G_{\mathrm{dock}}^{\mathrm{NE}}$ is found to be 20.6 kcal mol^{-1}. The good theory–experiment comparison as shown in Fig. 3a supports our approach to the [ion]-independent nonelectrostatic free energy $\Delta G_{\mathrm{dock}}^{\mathrm{NE}}$.

I. Free energy components

Fig. 3b shows the docking free energy ΔG_{dock} and its components as functions of $[Mg^{2+}]$. The components include the entropic free energy ΔG_{S}, the Coulomb energy ΔG_{E} and the

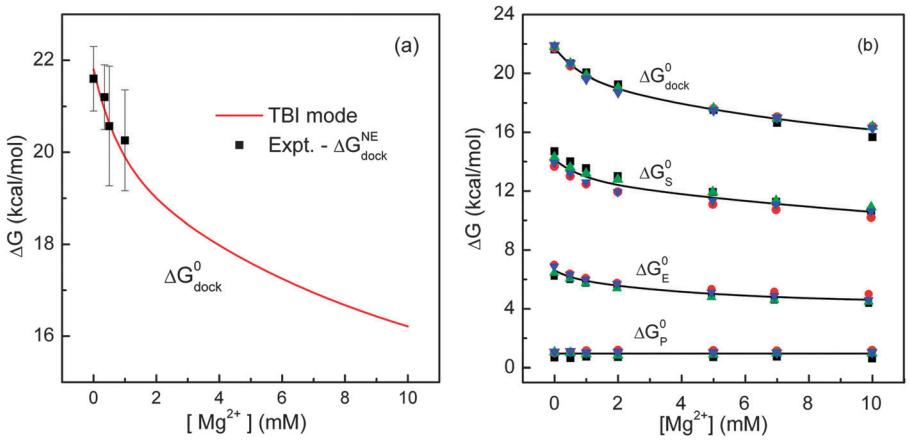

Fig. 3 The total docking free energy ΔG_{dock} and its components. (a) Comparison between the TBI-predicted electrostatic free energy for docking and (20.6 kcal mol^{-1} less than) the experimentally determined total docking free energy.[22] Here the free energy −20.6 kcal mol^{-1} accounts for the ion-independent (non-electrostatic) contribution $\Delta G_{\mathrm{dock}}^{\mathrm{NE}}$ in the tetraloop–receptor tertiary interaction. (b) The total docking free energy (ΔG_{dock}) and the corresponding component free energies as a function of the Mg^{2+} concentration in the background of 0.1 M NaCl at 37 °C. ΔG_{S}, ΔG_{E} and ΔG_{P} are respectively the entropic free energy, the Coulomb energy and the solvent polarization energy contributions.

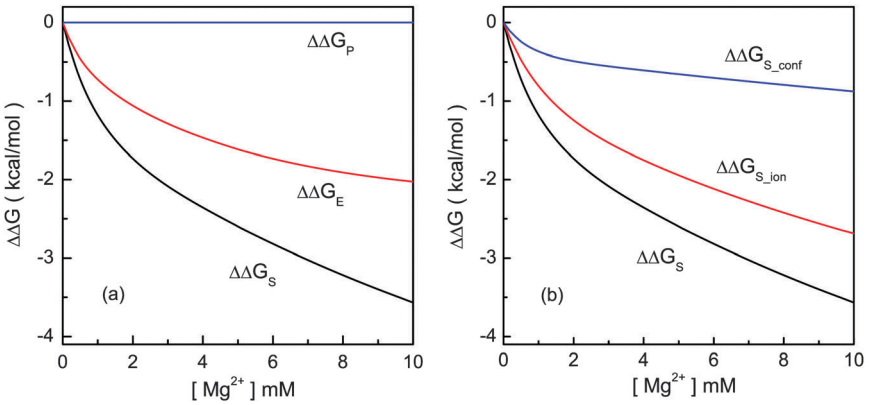

Fig. 4 (a) The Mg^{2+}-induced free energy changes: (a) the entropic free energy $\Delta\Delta G_S$, the Coulomb free energy $\Delta\Delta G_E$ and the polarization energy $\Delta\Delta G_P$; (b) the conformational entropy contribution $\Delta\Delta G_{S\_conf}$ and the ionic entropy contribution $\Delta\Delta G_{S\_ion}$.

polarization energy ΔG_P, each of which can be computed from eqn (1). The results shown in Fig. 3b include four sets of data from the four aforementioned Monte Carlo-generated conformational ensembles. The agreement between the four sets of results suggests that our Monte Carlo sampling may be reliable.

The different free energy components have different $[Mg^{2+}]$-dependence. Similar to the docking free energy ΔG_{dock}, the entropic free energy ΔG_S and the Coulomb energy ΔG_E decrease with increasing $[Mg^{2+}]$, while the polarization free energy ΔG_P remains nearly constant.

To further highlight the effect of Mg^{2+} ions in the docking process, we also calculate the Mg^{2+} ion-induced docking free energy change:[30]

$$\Delta\Delta G[Mg^{2+}] = \Delta G^{(obs)}[Mg^{2+}] - \Delta G^{(obs)}[0] \qquad (7)$$

where $\Delta G^{(obs)}[Mg^{2+}]$ and $\Delta G^{(obs)}[0]$ are the docking free energies with and without Mg^{2+} ions, respectively. As shown in Fig. 4a, $\Delta\Delta G_P$ remains nearly zero in the different $[Mg^{2+}]$, suggesting that Mg^{2+}does not cause significant changes in the solvent polarization effect in the docking process. Both the Coulombic free energy $\Delta\Delta G_E$ and the entropic free energy $\Delta\Delta G_S$ decrease with increasing $[Mg^{2+}]$, and $\Delta\Delta G_S$ decreases more rapidly than $\Delta\Delta G_E$. From 0 mM to 10 mM $[Mg^{2+}]$ at 37 °C, ΔG_E and ΔG_S decrease by about 2 kcal mol^{-1} and 3.5 kcal mol^{-1}, respectively, contributing about 40% and 60% to the total change of the docking free energy (5.6 kcal mol^{-1}). The main contribution comes from the entropic effect. The conclusion is in accordance with the experimental findings.[22]

II. Entropic effect

In our calculations, the entropic contribution is divided into two parts: the ion entropy contribution ΔG_{S_ion} and the conformational entropy contribution ΔG_{S_conf} (see Fig. 5a). To further clarify the effect of the different types of ions, we calculate the entropic free energies for the diffusive ($\Delta G_{S\_ion\_d}$) and the bound ions ($\Delta G_{S\_ion\_b}$) separately (see Fig. 5b).

Fig. 5 reveals several important features for the Mg^{2+}-induced entropic free energy changes. First, the entropic free energy of the diffusive ions ($\Delta G_{S\_ion\_d}$) is significantly larger than that of the bound ions ($\Delta G_{S\_ion\_b}$). Therefore, the ion entropy effect is dominated by the diffusive ions. Second, the entropic free energies ΔG_S, ΔG_{S_ion} and ΔG_{S_conf} decrease with increasing $[Mg^{2+}]$. Such a $[Mg^{2+}]$-dependence indicates Mg^{2+}-induced entropic forces in the stabilization of the docked state.

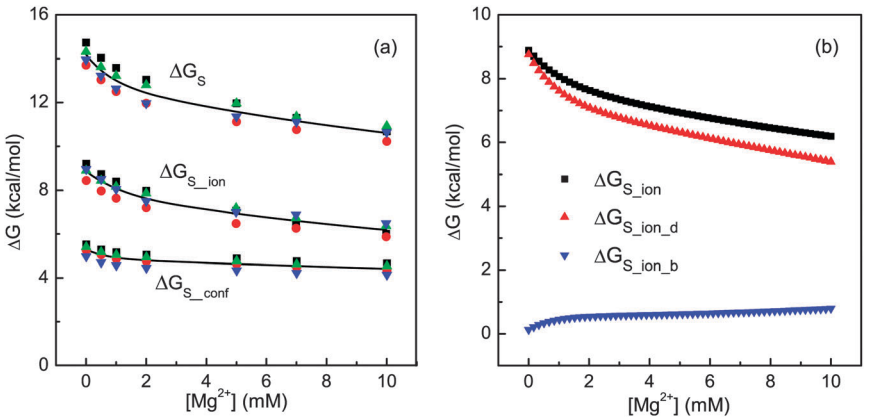

Fig. 5 The different components of the entropic free energy. (a) ΔG_{S_ion} and ΔG_{S_conf} are the free energies for the ion entropy and the conformational entropy, respectively. (b) The different components for the ion entropic free energies ΔG_{S_ion}: the diffusive ions $\Delta G_{S\_ion\_d}$ and the bound ions $\Delta G_{S\_ion\_b}$.

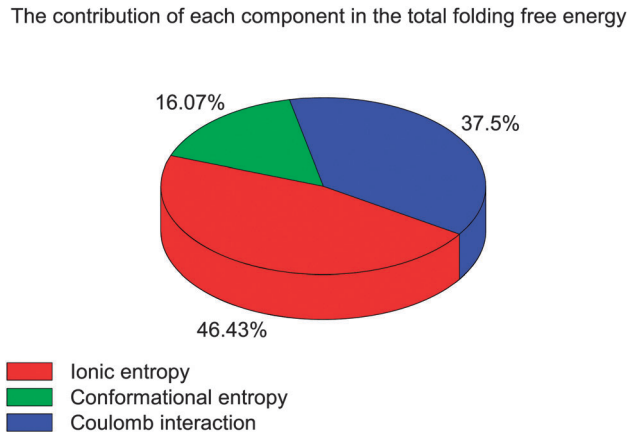

Fig. 6 The percentage of each component contribution in the total docking free energy at 10 mM [Mg^{2+}] with 0.1 M [Na^{+}] background at 37 °C.

Third, the changes of ΔG_{S_ion} and ΔG_{S_conf} from [Mg^{2+}] = 0 mM to [Mg^{2+}] = 10 mM are approximately 2.6 kcal mol^{-1} and 0.9 kcal mol^{-1} (shown in Fig. 5b), respectively. Then result shows that ion entropy (ΔG_{S_ion}) contributes nearly 75% of the net entropy change for the docking of the tetraloop–receptor system. Fourth, with increasing [Mg^{2+}], $\Delta G_{S\_ion\_d}$ decreases much faster than the total ionic contribution ΔG_{S_ion}, while $\Delta G_{S\_ion\_b}$, which gradually increases, shows an opposite trend. In Fig. 6, we show the percentage contribution of each component in the total docking free energy.

III. Ion uptake

We calculate the ensemble-averaged binding fraction f_b for both the docked and the undocked states. The uptake number for the docking is equal to

$$[f_b(F) - f_b(U)]\cdot N_a \quad (8)$$

where $f_b(F)$ and $f_b(U)$ are the binding fractions of the Mg^{2+} ions in the docked and the undocked states (see Fig. 7a) and N_a is the number of nucleotides in the RNA (N_a is 84 for the tetraloop–receptor system).

As shown in Fig. 7b, at [Mg^{2+}] = 0 mM, the uptake number of the counterions is about 0; with increasing [Mg^{2+}], the uptake number of ion rises and quickly reaches the maximum value ($\approx$1.7 at [Mg^{2+}] = 4.5 mM); when the [Mg^{2+}] further increases, the uptake number slowly decreases and becomes 1 at [Mg^{2+}] = 10 mM. This tendency is (qualitatively) consistent with the experimental measurements.[17,22,25]

IV. Bound ion distribution

To understand the bound ion distribution, we calculate the mean binding fraction on each nucleotide (see Fig. 8) for representative structures (see Fig. 10b for [Mg^{2+}] = 1 mM, Fig. 10c for 5 mM and Fig. 10d for 10 mM). The results show that the bound ions mainly distribute in the grooves of the helices. In addition, we find that the binding fraction on the receptor increases notably with increasing [Mg^{2+}], while the binding fraction on the tetraloop is relatively small, especially at low [Mg^{2+}].

Discussion

I. Docking free energy

The tetraloop–receptor docked complex involves significant tertiary interactions, such as hydrogen bonding and base stacking interactions between the tetraloop and the receptor.[17] The tertiary contacts can drastically decrease the free energy of the docked state. For example, the net free energy difference between the docked and the undocked states is no more than 1 kcal mol^{-1} under certain conditions ([Mg^{2+}] < 0.35 mM, [Na^{+}] = 100 mM and 37 °C)[19,22] suggesting significant cancellation between the electrostatic interactions and the (non-electrostatic) tertiary contacts. In the current analysis, we focus on the electrostatic free energy because our primary goal is to understand the role of ions. If invoking a transition-state analysis, the free energy difference between the transition state and the undocked states (the free energy barrier of docking) is about 17 kcal mol^{-1} under the same solution conditions.[22,25,26] Here, in the transition state the tetraloop and receptor are assumed to be in close

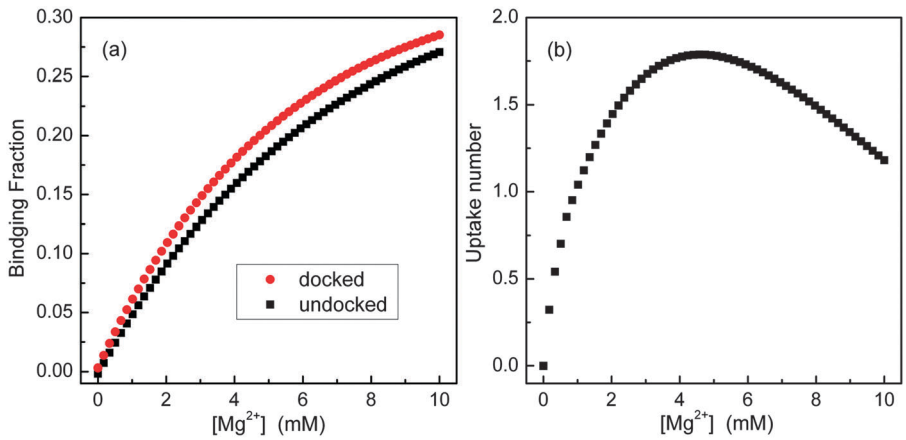

Fig. 7 (a) The binding fraction for the docked and the undocked states as a function of the Mg^{2+} concentration in the background of 0.1 M NaCl at 37 °C. (b) The uptake number of Mg^{2+}as a function of [Mg^{2+}].

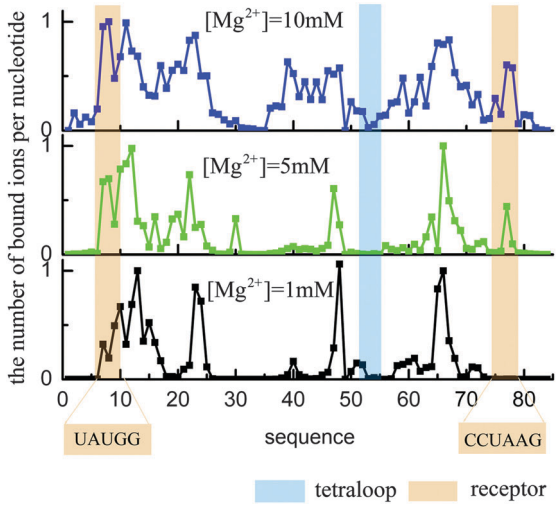

Fig. 8 The ion distribution for the lowest energy tetraloop–receptor structure (see Fig. 10b–d) in the different Mg^{2+} concentrations with 0.1 M NaCl background at 37 °C. The distribution is calculated as the Boltzmann average over all the possible ion binding models for the given RNA structure.

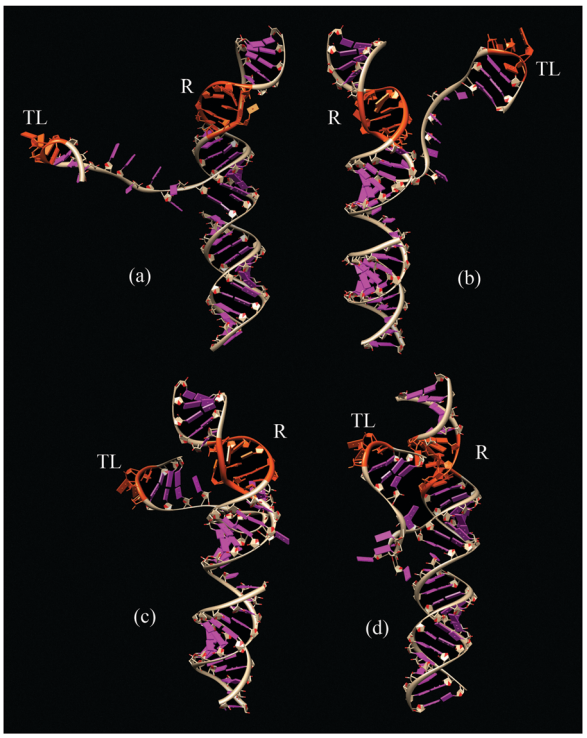

Fig. 10 The undocked structures with the lowest electrostatic free energy in the different Mg^{2+} concentrations with the fixed background of 0.1 M NaCl: (a) 0 mM, (b) 1 mM, (c) 5 mM and (d) 10 mM.

proximity, but the tertiary interactions are largely unformed.[22] Experimental data further suggest that the free energy barrier of docking mainly comes from the entropic effect.[22]

In our calculation, we focus on the ion-dependent electrostatic free energies, and the theory does not account for the tetraloop–receptor tertiary interaction energies. Therefore, effectively, our predicted electrostatic docking free energy reflects the difference between the undocked state and a special state. In this special state, the tetraloop–receptor native conformation has formed but the tertiary interactions have not yet established. Except for the conformational change of the receptor, this special state is close to the proposed transition state.[22] Therefore, the theoretical prediction for the docking free energy is comparable to the experimental result for the free

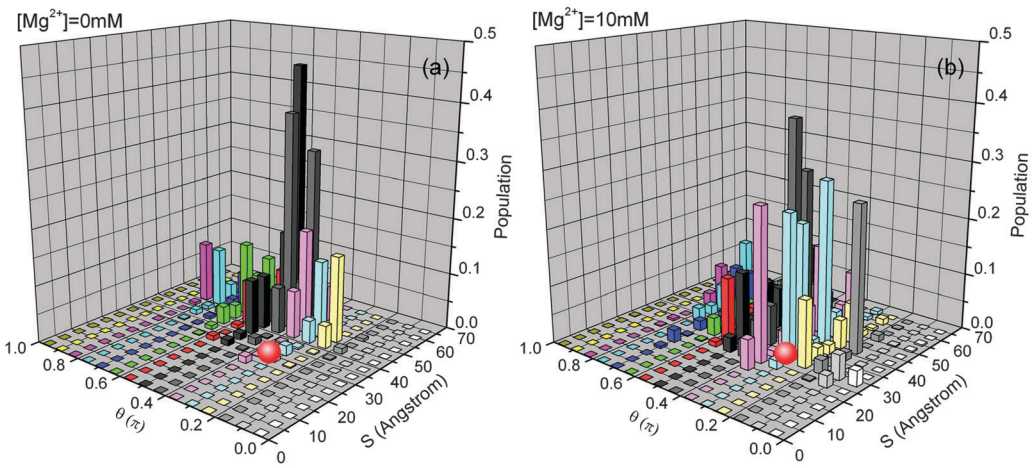

Fig. 9 The conformational distribution of the undocked state in the different Mg^{2+} concentrations with 0.1 M NaCl background at 37 °C. The calculation is based on the 4 sets independent Monte Carlo generated conformational ensembles. The figure shows the trend for the change of the populational distribution with increasing [Mg^{2+}] according to the structural parameters S (x axis) and θ (y axis) (shown in Fig. 1). The docked state (the red ball) is shown for reference. To calculate the population distribution, we first uniformly divide the conformational space into 30 clusters according to the distance S (see Fig. 1), we then uniformly divide each cluster into 30 sub-regions according to the angle θ (see Fig. 1). We calculate the average electrostatic free energy for the conformations in each subspace (S, θ) using the formula $\Delta G_{S,\theta} = \left(\sum_i \Delta G_i \cdot e^{-\Delta G_i/kT}\right) \Big/ \left(\sum_i e^{-\Delta G_i/kT}\right)$, where ΔG_i is the free energy of the ith conformation in subspace (S, θ). The z-axis in the figure shows the population of each subspace: ($P(S,\theta)$ = exp[$-(\Delta G_{S,\theta} - \Delta G_{min})/kT$]), where ΔG_{min} is the minimum electrostatic free energy in the whole space.

energy difference between the transition state and the undocked state. Our predicted docking free energies are higher than the experimental results and the difference is nearly independent of $[Mg^{2+}]$. For example, in 1 mM Mg^{2+} and 100 mM Na^{+} mixed solution at 37 °C, our calculated (electrostatic) docking free energy is about 20.3 kcal mol^{-1}. The experimentally measured free energy is about 0.34 kcal mol^{-1} for the net docking free energy and about 16 kcal mol^{-1} for the kinetic barrier. There is about a 4 kcal mol^{-1} difference between the predicted (electrostatic) docking free energy and the measured kinetic barrier.[22] Moreover, we find this free energy difference is nearly independent of $[Mg^{2+}]$. We propose the difference may come from two sources.

The tertiary structure of the docked tetraloop–receptor can form significant hydrogen bonding and base stacking.[17,37,38] Some hydrogen bonds may have already formed in the transition state, which lowers the free energy barrier. This may be a major reason causing the 4 kcal mol^{-1} difference. Furthermore, the receptor can be more flexible in the undocked state than in the docked state, causing an additional entropy cost.

In our model, the tetraloop and receptor structures are assumed to be fixed (PDB) structures. However, the receptor loop can be flexible in the undocked state. The flexible receptor becomes rigid in the docked state. Neglecting this additional conformational entropy change can also contribute to the 4 kcal mol^{-1} difference.[22,38]

Despite the difference between the predicted docking free energy and the experimental data for the free energy barrier, the $[Mg^{2+}]$-independent nonelectrostatic 4 kcal mol^{-1} difference does not change our results on the (electrostatic) $[Mg^{2+}]$-dependence of the docking free energy and the different free energy components.

II. Effect of ion entropy

Consistent with the experimental analyses,[22] our results (Fig. 3b and 4) suggest that the ion entropy provides the major force for Mg^{2+}-facilitated docking. Furthermore, by dissecting the ion entropy into diffusive and bound ion contributions, we found that the entropic force for tetraloop–receptor docking predominantly comes from the diffusive ions (Fig. 5b).

Fig. 5b shows that $\Delta G_{S\_ion\_b}$, the contribution from the entropy of the bound ions to the docking free energy, gradually increases with $[Mg^{2+}]$ and tends to stabilize at high $[Mg^{2+}]$. This result suggests that entropically, $\Delta G_{S\_ion\_b}$ opposes docking. More ions are bound to the docked state due to the higher RNA charge density in the (more compact) docked state than the undocked state, causing a net decrease in the entropy for the bound ions and hence an increase in the entropic free energy $\Delta G_{S\_ion\_b}$. The effect becomes weaker with increasing $[Mg^{2+}]$ because the entropy loss for ion binding becomes smaller in higher $[Mg^{2+}]$. Moreover, in a high $[Mg^{2+}]$ solution, both the undocked and the docked states involve significant charge neutralization, thus the increase in the number of bound ions in the docking process is limited. In contrast, in a low $[Mg^{2+}]$ solution, docking would induce a significant uptake of counterions (see Fig. 7).

Compared to the bound ions, the entropy of the diffusive ions promotes the docking process (Fig. 5b). With increasing $[Mg^{2+}]$, more cations bind to the RNA molecule, causing stronger charge neutralization. RNA charge neutralization leads to a more uniform distribution (large entropy) of the diffusive ions. The larger entropy of the diffusive ions lowers the free energy of the system. This effect is more pronounced for the docked state than for the undocked state due to the stronger charge neutralization effect in the docked state. Furthermore, a higher $[Mg^{2+}]$ (<5 mM) leads to an increased Mg^{2+} ion uptake and Na^{+} ion release, causing an increase in Na^{+} ion entropy. Therefore, the diffusive ion entropy promotes the tetraloop–receptor docking. This conclusion agrees with the analysis based on the experimental data.[22]

III. Conformational entropy effect

Fig. 6 shows that the conformational entropy occupies a small fraction of the docking free energy. Furthermore, Fig. 4b shows that the Mg^{2+} can induce a stabilizing force from the conformational entropy. As shown in Fig. 9, a higher $[Mg^{2+}]$ causes a higher probability for the close approach (small S) between the tetraloop and the receptor. The overall conformational distribution is shifted toward the more compact state in the vicinity of the docked structure (denoted by a red ball in Fig. 9). Indeed, as shown in Fig. 10, the low free energy conformations become more compact in higher $[Mg^{2+}]$. Thus, from the point of view of the conformational entropy, increasing $[Mg^{2+}]$ tends to stabilize the docked state.

IV. Effect of Coulomb interaction

In our calculation, the change of the Coulomb free energy ΔG_E from $[Mg^{2+}] = 0.35$ mM to $[Mg^{2+}] = 1$ mM is about 0.7 kcal mol^{-1}. This value is within the error bar of the experimental measurement.[22] A similar viewpoint for the minor difference of the Coulomb energy between the experimental data and theoretical calculations was also reported for DNA systems.[50–52]

The Coulomb energy effect in the docking process can stem from several Coulomb effects. First, ions can neutralize RNA backbone charge to reduce Coulomb repulsion between the tetraloop and the receptor. Second, Mg^{2+} ions can promote docking through the Coulomb correlation effect. For a compact (docked) structure, compared to the undocked structure, the higher negative charge density of the RNA would cause significant ion binding and thus high concentration of counterions around the RNA surface. The high concentration of counterions leads to strong correlation (coupling) between ions. In the docking process, the (correlated) Mg^{2+} ions bound to the tetraloop part (including the connected helix stem) and those bound to the receptor part (including the connected helix stems) can self-organize to reach a low correlated Coulomb energy, and such a low-energy state is beyond the charge neutralization effect. This Coulomb correlation effect can add an additional Coulomb effect to promote the docking by lowering the Coulomb energy of the system.

Conclusion

Using a physics-based RNA folding model (Vfold) to sample the conformations of the flexible loop in 3D space, we generate the conformational ensembles of both the docked and the undocked states. Using the TBI theory for ion–RNA interactions, we predict the electrostatic thermodynamics of the tetraloop–receptor system in a salt solution with the different [Mg^{2+}]. The docking free energy landscape and the component contributions demonstrate that the ion entropy provides the major stabilizing force for tetraloop–receptor docking. Further detailed theoretical analysis indicates that the dominant contribution to the ion entropy force comes from the redistribution of the diffusive ions. Through the electrostatic screening/charge neutralization effect, the Coulomb force can also play a (*albeit* minor) role in the docking process. The predicted results are consistent with the experimental data and analysis. The method presented here may provide a paradigm for studying the folding of more complex RNA structures.

Acknowledgements

This research was supported by NSF grants MCB0920067 and MCB0920411 and NIH grant GM063732. Most of the computations in this research were performed on the HPC resources at the University of Missouri Bioinformatics Consortium (UMBC).

References

1 C. D. Downey, J. L. Fiore, C. D. Stoddard, J. H. Hodak, D. J. Nesbitt and A. Pardi, *Biochemistry*, 2006, **45**, 3664.
2 P. Z. Qin, S. E. Butcher, J. Feigon and W. L. Hubbell, *Biochemistry*, 2001, **40**, 6929.
3 J. H. Davis, M. Tonelli, L. G. Scott, L. Jaeger, J. R. Williamson and S. E. Butcher, *J. Mol. Biol.*, 2005, **351**, 371.
4 M. Maderia, T. E. Horton and V. J. DeRose, *Biochemistry*, 2000, **39**, 8193.
5 J. H. Davis, T. R. Foster, M. Tonelli and S. E. Butcher, *RNA*, 2007, **13**, 76.
6 X. Qiua, V. A. Parsegian and D. C. Rau, *Proc. Natl. Acad. Sci. U. S. A.*, 2010, **107**, 21482.
7 S. Kirmizialtin, S. A. Pabit, S. P. Meisburger, L. Pollack and R. Elber, *Biophys. J.*, 2012, **102**, 819.
8 A. A. Chen, M. Marucho, N. A. Baker and R. V. Pappu, *Methods Enzymol.*, 2009, **469**, 411.
9 S. Hamill and A. M. Pyle, *Mol. Cell*, 2006, **23**, 831.
10 C. D. Downey, R. L. Crisman, T. W. Randolph and A. Pardi, *J. Am. Chem. Soc.*, 2007, **129**, 9290.
11 M. l. C. Erat and R. K. O. Sigel, *Inorg. Chem.*, 2007, **46**, 11224.
12 A. Laederach, I. Shcherbakova, M. A. Jonikas, R. B. Altman and M. Brenowitz, *Proc. Natl. Acad. Sci. U. S. A.*, 2007, **104**, 7045.
13 J. L. Fiore, J. H. Hodak, O. Piestert, C. D. Downey and D. J. Nesbitt, *Biophys. J.*, 2008, **95**, 3892.
14 R. Ishitani, S. Yokoyama and O. Nureki, *Curr. Opin. Struct. Biol.*, 2008, **18**, 330.
15 X. Qu, G. J. Smith, K. T. Lee, T. R. Sosnick, T. Pan and N. F. Scherer, *Proc. Natl. Acad. Sci. U. S. A.*, 2008, **105**, 6602.
16 K. A. Vander Meulen, J. H. Davis, T. R. Foster, M. T. Record Jr. and S. E. Butcher, *J. Mol. Biol.*, 2008, **384**, 702.
17 J. L. Fiore, B. Kraemer, F. Koberling, R. Edmann and D. J. Nesbitt, *Biochemistry*, 2009, **48**, 2550.
18 Y. Zhang, X. Zhao and Y. Mu, *J. Chem. Theory Comput.*, 2009, **5**, 1146.
19 A. J. DePaul, E. J. Thompson, S. S. Patel, K. Haldeman and E. J. Sorin, *Nucleic Acids Res.*, 2010, **38**, 4856.
20 C. D. Duncan and K. M. Weeks, *PLoS One*, 2010, **5**, e8983.
21 S. A. Woodson, *Annu. Rev. Biophys.*, 2010, **39**, 61.
22 J. L. Fiore, E. D. Holmstrom and D. J. Nesbitt1, *Proc. Natl. Acad. Sci. U. S. A.*, 2012, **109**, 2902.
23 K. A. Vander Meulen and S. E. Butcher, *Nucleic Acids Res.*, 2012, **40**, 2140.
24 P. Z. Qin, J. Feigon and W. L. Hubbell, *J. Mol. Biol.*, 2005, **351**, 1.
25 E. D. Holmstrom, J. L. Fiore and D. J. Nesbitt, *Biochemistry*, 2012, **51**, 3732.
26 J. L. Fiore, E. D. Holmstrom, L. R. Fiegland, J. H. Hodak and D. J. Nesbitt, *J. Mol. Biol.*, 2012, **423**, 198.
27 J. H. Hodak, C. D. Downey, J. L. Fiore, A. Pardi and D. J. Nesbitt, *Proc. Natl. Acad. Sci. U. S. A.*, 2005, **102**, 10505.
28 J. C. Bowman, T. K. Lenz, N. V. Hud and L. D. Williams, *Curr. Opin. Struct. Biol.*, 2012, **22**, 262.
29 D. Leipply and D. E. Draper, *Biochemistry*, 2010, **49**, 1843.
30 D. Grilley, A. M. Soto and D. E. Draper, *Proc. Natl. Acad. Sci. U.S.A.*, 2006, **103**, 14003.
31 P. T. Li, J. Vieregg and I. Tinoco Jr., *Annu. Rev. Biochem.*, 2008, **77**, 77.
32 D. E. Drape, D. Grilley and A. Soto, *Annu. Rev. Biophys. Biomol. Struct.*, 2005, **34**, 221.
33 I. Tinoco Jr and C. Bustamante, *J. Mol. Biol.*, 1999, **293**, 271.
34 H. Heus and A. Pardi, *Science*, 1991, **253**, 191.
35 M. Costa and F. o. Michel, *EMBO J.*, 1995, **14**, 1276.
36 F. M. Jucer and A. Pardi, *RNA*, 1995, **1**, 219.
37 J. H. Cate, A. R. Gooding, E. Podell, K. Zhou, B. L. Golden, C. E. Kundrot, T. R. Cech and J. A. Doudna, *Science*, 1996, **273**, 1678.
38 S. E. Butcher, T. Dieckmann and J. Feigon, *EMBO J.*, 1997, **16**, 7490.
39 A. S. Krasilnikov, X. Yang, T. Pan and A. Mondragón, *Nature*, 2003, **421**, 760.
40 J. H. Davis, M. Tonelli, L. G. Scott, L. Jaeger, J. R. Williamson and S. E. Butcher, *J. Mol. Biol.*, 2005, **351**, 371.
41 S. Cao and S. J. Chen, *Nucleic Acids Res.*, 2012, **40**, 4681.
42 S. Cao and S. J. Chen, *RNA*, 2011, **17**, 2130.
43 S. Cao and S.-J. Chen, *Nucleic Acids Res.*, 2006, **34**, 2634.
44 Z.-J. Tan and S.-J. Chen, *Met. Ions Life Sci.*, 2011, **9**, 101.
45 Z. J. Tan and S. J. Chen, *Biophys. J.*, 2011, **101**, 176.
46 Z. J. Tan and S. J. Chen, *Biophys. J.*, 2008, **94**, 3137.
47 Z. J. Tan and S. J. Chen, *Biophys. J.*, 2007, **92**, 3615.
48 Z. J. Tan and S. J. Chen, *J. Chem. Phys.*, 2005, **122**, 44903.
49 Z. He and S.-J. Chen, *J. Chem. Theory Comput.*, 2012, **8**, 2095.
50 S. G. Delcourt and R. D. Blake, *J. Biol. Chem.*, 1991, **266**, 15160.
51 D. Erie, N. Sinha, W. Olson, R. Jones and K. Breslauer, *Biochemistry*, 1987, **26**, 7150.
52 V. K. Misra and D. E. Draper, *J. Mol. Biol.*, 1999, **294**, 1135.